Water Air Soil Pollut (2017) 228: 387
DOI 10.1007/s11270-017-3579-y

Cry1Ab Adsorption and Transport in Humic Acid-Coated Geological Formation of Alumino-Silica Clays

Hongying Yuan · Simeng Li · Junliang Liu · Chengyi Song · Gang Chen

Received: 12 June 2017 / Accepted: 12 September 2017 / Published online: 20 September 2017

Abstract Genetically modified agricultural products have been introduced to increase food supply by enhancing their resistance to pests and diseases, along with easily adapting to environmental conditions. Due to the modification of DNA, public objections are prevalent, including concerns on the impact on the ecosystem. In this research, adsorption and transport of Cry1Ab, a toxin exuded by the transgenic *Bt* maize in alumino-silica clays, were evaluated in laboratory columns under steady-state flow conditions. Since Cry1Ab fate and transport were very responsive to animal waste field applications, during which humic acids were released, Cry1Ab adsorption and transport in humic acid-coated alumino-silica clays were also investigated. Cry1Ab breakthrough curves were simulated using the convection-dispersion transport models. It was discovered that the humic acid coating increased Cry1Ab deposition during the transport. Based on analysis of the breakthrough curves, adsorption isotherms of Cry1Ab in alumino-silica clays were obtained and compared with those of batch experiments. The humic acid coating changed the bonding energy between Cry1Ab and the adsorption receptor sites on alumino-silica clay surfaces, thereby changing Cry1Ab partition between the aqueous phase and the solid phase.

Keywords Cry1Ab · Humic acid · Alumino-silica clay · Transport · Adsorption

H. Yuan · J. Liu
Department of Urban Construction, Hebei University of Agriculture, Baoding, China

S. Li · G. Chen
Department of Civil and Environmental Engineering, Florida State University, Tallahassee, FL, USA

C. Song
Department of Water Engineering and Sciences, Hunan University, Changsha, China

G. Chen (✉)
Department of Civil and Environmental Engineering, FAMU-FSU College of Engineering, 2525 Pottsdamer Street, Tallahassee, FL 32310, USA
e-mail: gchen@eng.fsu.edu

1 Introduction

Genetically modified agricultural products have been introduced in the agricultural system and on the market of consumer goods in the last 10 to 20 years (Lehrman and Johnson 2008; Wheatley 2009). Owing to the potential to modify the DNA of living organisms, there are extensive discussion and controversy regarding genetic engineering applications in agricultural practices (Uzogara 2000). Public objections have numerous causes, including the impact on the ecosystem (Barton and Dracup 2000; Carstens et al. 2012; Loureiro et al. 2009; Peterson et al. 2000; Wheatley 2009). Transgenic *Bt* maize is one of the most extensively studied examples, which is genetically modified with genes from *Bacillus thuringiensis* (*Bt*), a naturally occurring ubiquitous soil bacterium. Transgenic *Bt* maize plants express toxins against lepidopteran (Cry1Ab protein), which may eventually impact the ecosystem.

The fate of Cry1Ab, as a toxin in the soil, is an important consideration for soil and groundwater contaminations. It has been demonstrated that *Bt* plants exude Cry1Ab from their roots during their entire life cycle. Cry1Ab is also released from dead plant material into the soil (Helassa et al. 2011). Besides, *Bt*-corn pollen is also the potential source of *Bt* proteins that can be introduced to the soil of both the designated farming land of genetically modified crops and adjacent land. Available data indicate that the half-life of Cry1Ab incorporated into the soil is 1.6 to 22 days but can be as long as 46 days (Clark et al. 2005). These numbers vary considerably based on soil characteristics. Laboratory and field studies have demonstrated that degradation of Cry1Ab in agricultural soils can be carried out by soil microorganisms (Fu et al. 2012; Lutz et al. 2006) and Cry1Ab causes no or only minor changes in microbial community structure, which is often transient in duration (Clark et al. 2005). Cry1Ab fate is very responsive to agricultural practices including animal waste field applications. Depending on different agricultural practices, Cry1Ab might cause a longer persistence and subsequent accumulation in the soil or water.

Animal waste is considered a valuable resource, which, when managed properly, can reduce the need for commercial fertilizer. Animal waste can add organic matter to improve the soil water holding capacity and tilth (Ma et al. 1998). It also provides an economical source of nitrogen, phosphorus, and potassium as well as other nutrients needed for plant growth. Currently, it is well-recognized that land applications are the best method of utilizing animal manure. Animal waste field applications would lead to the release of humic acids, which can combine with metal ions, oxides, and clay minerals to form water soluble or insoluble complexes and thus affect Cry1Ab transport in the soil.

In order to assess the impact of genetically modified agricultural practices on the ecosystem, the fate and transport of Cry1Ab in the subsurface soil should be investigated. Especially, with popular animal waste field applications, humic acids would release and coat the soil media surface, which thereby changes Cry1Ab adsorption in the agricultural soil. In this research, it was hypothesized that Cry1Ab protein persisted in the soil and its fate and transport depended on agricultural field practices such as animal waste applications. The objectives of this research were to evaluate Cry1Ab adsorption and transport in the subsurface soil under animal waste field applications. Geological formation of alumino-silica clays was used as model media, and Cry1Ab transport was evaluated in laboratory columns under steady-state flow conditions with humic acid-coated alumino-silica clays. Cry1Ab breakthrough curves were simulated using the convection-dispersion transport models, and simulated adsorption transport parameters were interpreted based on the results of batch adsorption isotherms.

2 Materials and Methods

Purified Cry1Ab protein was purchased from MyBioSource, Inc. (San Diego, CA). Hydrolysis of Cry1Ab was first evaluated by dissolving Cry1Ab in 0.1 M phosphate buffer at a concentration of 500 ng/mL and pH 6 and 7. The solution was transferred into screw-cap glass test tubes and incubated at 25 °C in the dark. At different time intervals, Cry1Ab was sampled and the concentration was analyzed by enzyme-linked immunosorbent assay (ELISA) with a QuantiPlate kit (AP 003, Envirologix, Portland, ME) at 450 nm (SpectraMax 190, Molecular Devices, Sunnyvale, CA). The above experiments were performed in triplicate.

The mineralogical alumino-silica clays of zeolite (ZK406H, ZS403H, and ZS500H) (obtained from St. Cloud Mining Co., Winston, NM) were used as model media in this research. The zeolite type of ZK406H and ZS403H is clinoptilolite, and the zeolite type of ZS500H is chabazite. The average geometric mean grain size of the zeolite used for this research was 2.54 mm, and the specific surface areas were 531.7, 546.4, and 478.6 m^2/g for ZK406H, ZS403H, and ZS500H, respectively, as determined by BET gas adsorption using N_2 (ASAP2010, Micromeritics, Norcross, GA). The bulk densities were 0.97, 1.12, and 0.85 g/cm^3, and the ion exchange capacities were 1.54, 1.76, and 2.21 meq/g for ZK406H, ZS403H, and ZS500H, respectively. Bulk density linked Cry1Ab adsorption in zeolite to its aqueous concentration, thus playing an important role in Cry1Ab adsorption. After rinsing using deionized water, the zeolite clays were treated with sodium acetate, hydrogen peroxide, sodium dithionate, and sodium citrate to remove impurities such as organic matter.

Humic acids were extracted from dairy manure collected from a dairy farm located 1 mi south of the city of Mayo, Florida. The manure was first mixed with deionized water with pH adjusted to 12 with NaOH. After shaking for 1 h, the manure solution was filtered by a

0.45-μm filter. The pH of the filtrate was lowered with HCl, and the precipitates were collected and dried as extracted humic acids. Zeolite was coated by the humic acids as described below. The humic acids were added with 0.1 M NaOH, mixed with zeolite (1: 5 *w*/*w*) in 0.01 M $NaNO_3$ solution (pH 7.5), and shaken for 48 h. Coated zeolite was then washed with 0.1 M $NaNO_3$ (pH 7.0) via centrifugation. After rinsing with de-ionized water, coated zeolite was oven-dried at 110 °C. The amount of humic acids coated on zeolite was determined by detachment of the humic acids in 1 M NaOH followed by quantification with UV-vis spectrometry (Agilent Technologies Cary 60) at a wavelength of 254 nm. The spectroscopic measurements were calibrated with a TOC analyzer (Shimadzu TOC 5000). The amount of humic acids that could be coated onto the three zeolite clays was around 1 mg/g.

2.1 Cry1Ab Adsorption Isotherm

Batch isotherms were conducted to determine Cry1Ab adsorption in zeolite and humic acid-coated zeolite. A series of 25-mL vials containing Cry1Ab solutions (20 mL) at the concentrations of 50, 100, 150, 250, 400, and 500 ng/mL in 0.1 M phosphate buffer (to help maintain a constant pH of the solution) and 50-mg zeolite or humic acid-coated zeolite as well as blank controls (sealed with Teflon-lined screw caps) were agitated on a wrist action shaker (Burrel Scientic, Model 75) to reach equilibrium, i.e., the amount of the Cry1Ab in the supernatant remained constant with time. 0.1 mL of $CHCl_3$ was added to prevent microbial activities. The suspension was then centrifuged at 12,000×*g* for 15 min, after which Cry1Ab concentration in the supernatant was measured by ELISA with the QuantiPlate kit. The amount of Cry1Ab adsorbed on zeolite or humic acid-coated zeolite was calculated based on the mass balance of the difference between the initial and equilibrated solutions. Three replicates were conducted for each sample.

2.2 Column Experiments

Column experiments were conducted to study the adsorption and transport of Cry1Ab in zeolite and humic acid-coated zeolite. The column experiments were conducted under saturated conditions with the column (5-cm ID × 15-cm length) vertically oriented. The bottom of the column was sealed with a custom fit to permit the flow of water and retain the zeolite clays. To pack the column with zeolite, the column was first filled with nanopure de-ionized water to a height of 2 to 3 cm and the zeolite was packed in the column through CO_2 solvation to eliminate air pockets. During packing, a height of 2 to 3 cm of nanopure de-ionized water was maintained. As mentioned before, the bulk densities were 0.97, 1.12, and 0.85 g/cm^3 for ZK406H, ZS403H, and ZS500H, respectively, once they were packed in the column. For each series of the column experiments, a fresh column was packed. To ensure a stabilized flow regime and eliminate the impurity, approximately 100 pore volumes of nanopure de-ionized water were eluted through the column by a peristaltic pump prior to each experiment (Masterflex, Cole-Parmer, Vernon Hills, IL). A conservative pulse tracer (chloride) breakthrough curve was generated separately before the introduction of Cry1Ab. For each column run, 135 mL of Cry1Ab at a concentration of 500 ng/mL in 0.1 M phosphate buffer of pH 7 (in the presence of 0.005 mL/mL of $CHCl_3$ to prevent microbial activities) was introduced to the column at a flow rate of 1.5 mL/min, after which the column was continuously flushed with nanopure de-ionized water until the background signal was detected from the elution collected by a fraction collector. The collected elution was measured for Cry1Ab as described before. For each column experiment, three runs were performed, and the inconsistency of breakthrough curves was within 5% (95% CI).

Under saturated conditions, Cry1Ab transport was controlled by kinetic adsorption and equilibrium adsorption processes. Cry1Ab transport can thus be described by (Bai et al. 1997)

$$\theta\frac{\partial}{\partial t}C+\rho_b\frac{\partial S}{\partial t}=\frac{\partial}{\partial z}\left[\theta D_z\frac{\partial C}{\partial z}\right]-\frac{\partial}{\partial z}[qC]-\theta k_1 C \qquad (1)$$

$$\frac{\partial C_r}{\partial t}=k_1\frac{1}{\rho_b}C \qquad (2)$$

where C is the Cry1Ab concentration in the solution; ρ_b is the media bulk density; S is the adsorbed Cry1Ab that is in equilibrium with the Cry1Ab in the solution; D_z is the apparent dispersion coefficient, which is estimated from Pe, i.e., $D_Z=\frac{vL}{Pe}$ (L is the length of the column, and v is interstitial pore water velocity); q is the specific discharge (Darcian fluid flux); k_1 is the deposition coefficient; θ is the porosity; C_r is the kinetically adsorbed

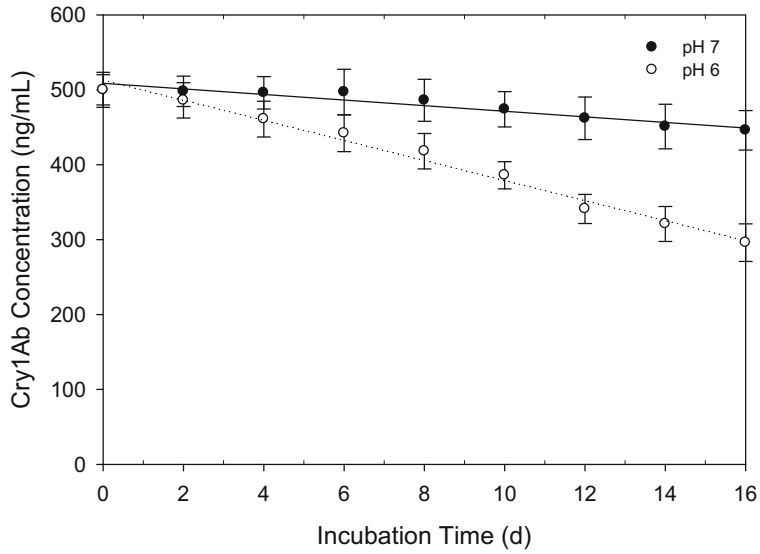

Fig. 1 Hydrolysis of Cry1Ab as a function of time

Cry1Ab; z is the axial coordinate; and t is the time. If the equilibrium adsorption (i.e., reversible adsorption) of Cry1Ab is assumed to be linear, then

$$\frac{\partial S}{\partial t} = \frac{\partial S}{\partial C}\frac{\partial C}{\partial t} = K_p \frac{\partial C}{\partial t} \tag{3}$$

where K_p is the partition coefficient of Cry1Ab between the aqueous phase and zeolite clays. By substituting Eq. (3) into Eq. (1), Eq. (1) becomes

$$\left(1 + \frac{\rho_b K_p}{\theta}\right)\frac{\partial C}{\partial t} = \frac{\partial}{\partial z}\left[D_z \frac{\partial C}{\partial z}\right] - \frac{\partial}{\partial z}\left[\frac{q}{\theta} C\right] - k_1 C \tag{4}$$

Defining $(1 + \frac{\rho_b K_p}{\theta})$ as the retardation factor, R, Eq. (4) is simplified as

$$R\frac{\partial}{\partial t} C = \frac{\partial}{\partial z}\left[D_z \frac{\partial C}{\partial z}\right] - \frac{\partial}{\partial z}\left[\frac{q}{\theta} C\right] - k_1 C \tag{5}$$

The above models are only valid if the media surface coverage by Cry1Ab was low. In this research, a fresh column was used for each Cry1Ab transport experiment. Therefore, the media surface coverage remained very low. Subsequently, above equations should be valid to be utilized to describe Cry1Ab transport. During simulation, a pulse-type boundary condition was used for the upper boundary and a zero gradient was assumed for the lower boundary (Reed 1965):

$$\left[-\theta D_z \frac{\partial C}{\partial z} + qC\right]_{z=0} = \left\{\begin{matrix} qC_0 & at & 0 < t \le t_0 \\ 0 & at & t > t_0 \end{matrix}\right\} \tag{6}$$

$$\left.\frac{\partial C}{\partial z}\right|_{z=L} = 0 \tag{7}$$

where t_0 is the duration of injection and C_0 is the initial Cry1Ab concentration.

3 Results and Discussion

Based on the Western blot analysis, 90% of the Cry1Ab protein had a molecular size of 65 kDa. Fragmented Cry1Ab protein included 5% in the size of 34 kDa and 5% in the size of 17 kDa. The zeta potential of Cry1Ab at pH 7 was − 18.4 mV. Cry1Ab was relatively resistant to hydrolysis at a neutral pH of 7, indicating insignificant of abiotic degradation (Fig. 1). With the decrease of pH, hydrolysis of Cry1Ab increased, which displayed a linear relationship with incubation time. At pH of 6, hydrolysis of Cry1Ab was obvious with 16% hydrolyzed after 8 days and 40% hydrolyzed after 16 days. All the column experiments in this research were conducted at pH of 7 within 900 min. Therefore, Cry1Ab loss by hydrolysis could be ignored.

ZS500H had the greatest negative ζ-potential of − 31.3 mV, ZK406H had the smallest ζ-potential of

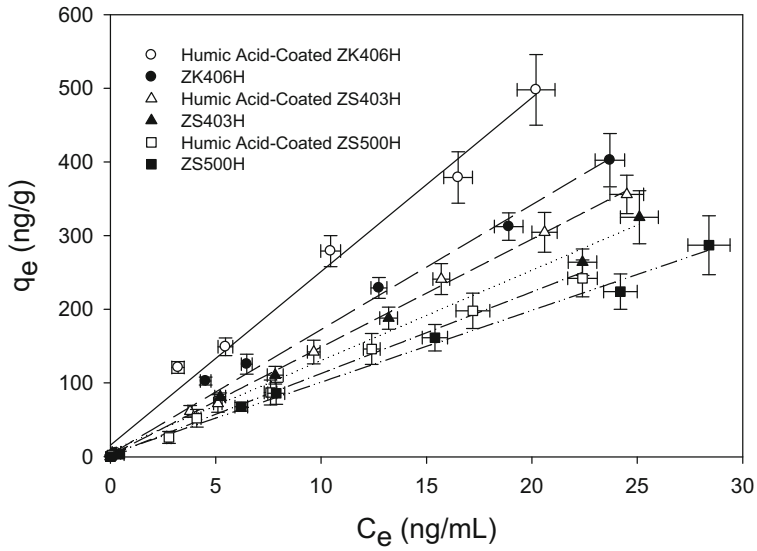

Fig. 2 Cry1Ab adsorption isotherms in zeolite clays and humic acid-coated zeolite

− 27.4 mV, and ZS403H was in between with a ζ-potential value of − 28.2 mV. Cry1Ab displayed a linear adsorption isotherm in ZK406H, ZS403H, and ZS500H, respectively. When equilibrium adsorption was reached, the partition coefficients of Cry1Ab between the aqueous phase and ZK406H, ZS403H, and ZS500H was 17, 13, and 10 mL/g, respectively. The adsorption of Cry1Ab in ZK406H, ZS403H, and ZS500H increased linearly with the increase of the equilibrium concentration up to 30 ng/mL (Fig. 2). Cry1Ab had the greatest adsorption in ZK406H, followed by ZS403H and ZS500H. Cry1Ab also displayed linear adsorption isotherm in humic acid-coated zeolite with partition coefficients of 25, 15, and 11 mL/g for ZK406H, ZS403H, and ZS500H, respectively.

Nearly all the input tracer was eluted from the column (Fig. 3). The tracer breakthrough curve was simulated with Eq. (1). During the model simulation, k_1 was set to 0. This was based on the consideration that chloride should not be retained in the media as chloride was assumed to not adsorb in the media. This is true since nearly all the inputted chloride was eluted from the column at the end of the tracer experiments. After the simulation, D_z was determined to be 11.2 cm^2/min, which was then used for all the simulations of Cry1Ab transport in

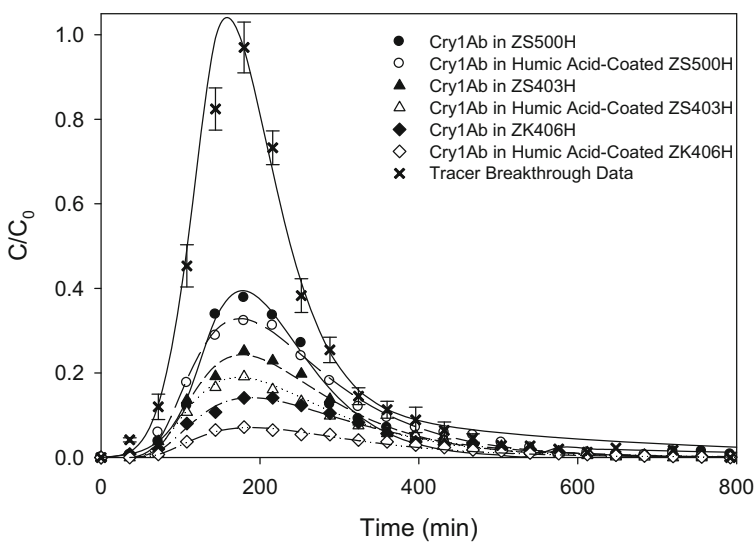

Fig. 3 Cry1Ab transport breakthrough curves in zeolite and humic acid-coated zeolite

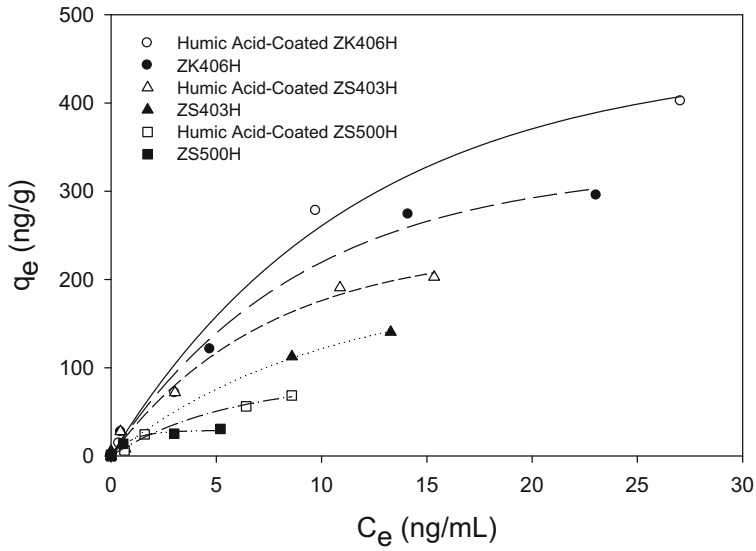

Fig. 4 Cry1Ab nonlinear adsorption isotherms simulated from breakthrough curves

zeolite clays. Breakthrough curves of Cry1Ab in ZK406H, ZS403H, and ZS500H were characterized by a self-sharpening front, which became broader and more diffuse at the elution limb (Fig. 3). The long-lasting tails of the breakthrough curves indicated kinetic-controlled Cry1Ab retention in the column. Under saturated conditions, Cry1Ab transport is controlled by kinetic adsorption and equilibrium adsorption processes, which has been proven to be true for solute transport in sand columns. Equations (1) and (2) were solved by using a finite-difference method with a predictor-corrector time-stepping scheme with a pulse-type boundary condition for the upper boundary and a zero gradient for the lower boundary. All the parameters were optimized by minimizing the sum of squared differences between observed and fitted concentrations using the nonlinear least-square method (Toride et al. 1995).

Cry1Ab displayed irreversible adsorption or kinetic adsorption in zeolite clays, which was evidenced by the reduced mass recovery during the transport. The kinetic adsorption was best described by the deposition coefficient. The humic acid coating increased Cry1Ab kinetic adsorption in zeolite clays. As shown in Fig. 3, as compared to uncoated zeolite clays, Cry1Ab had greater deposition in humic acid-coated zeolite clays (deposition coefficients of 4.31, 2.72, and 1.84 h^{-1} as compared to 3.21, 2.31, and 1.59 h^{-1} for ZK406H, ZS403H, and ZS500H, respectively). It was likely that the humic acid coating impacted zeolite surface properties. The increase of deposition of Cry1Ab in humic acid-coated zeolite clays was attributed to the coating of humic acids on the zeolite surfaces.

Although linear adsorption isotherms were discovered from batch experiments, nonlinear adsorption isotherms were suspected for Cry1Ab in zeolite clays. A method has been developed to allow rapid determination of nonlinear adsorption isotherms by integrating the diffuse front of the breakthrough curves (Burgisser et al. 1993). Based on this method, the concentration of reversibly adsorbed Cry1Ab in zeolite clays, *S*, can be obtained by integrating the

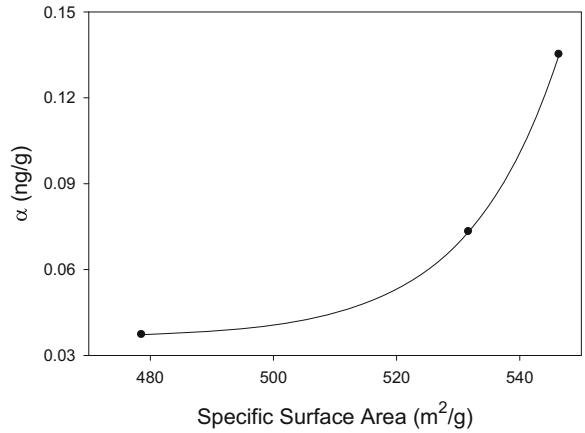

Fig. 5 Cry1Ab required to completely cover a unit mass of zeolite; α as a function of zeolite-specific surface area

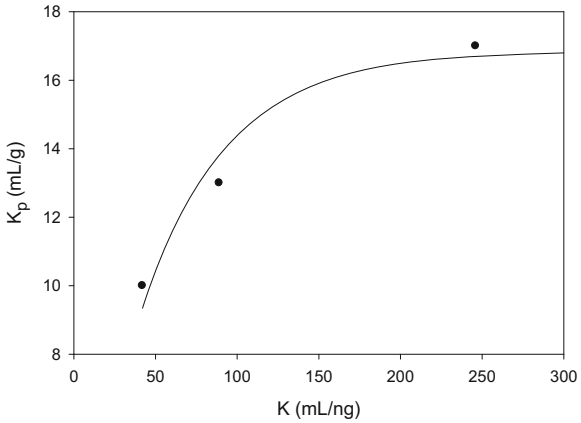

Fig. 6 Partition coefficient of Cry1Ab between the aqueous phase and zeolite clays, K_p, as a function of the Langmuir adsorption constant, K

experimental record of the retention time $t(c)$ if the dispersion term can be neglected ($D = 0$):

$$S = \frac{\theta}{\rho_b(1-\theta)} \int_0^c \left(\frac{t(c')}{t_0} - 1 \right) dc' - \int_0^c t(c') k_c dc' \tag{8}$$

where $t_0 = L/v$ and is the average Cry1Ab travel time in the column. The insignificant role of hydrodynamic dispersion on solute transport in a column has been proven to be valid (Unice and Logan 2000). It has been demonstrated that hydrodynamic dispersion can be neglected for $Pe > 100$. For this research, all the column experiments were performed with $Pe > 100$; thus, Eq. (8) can be used to determine the Cry1Ab adsorption isotherms.

Cry1Ab adsorption isotherms were obtained using Eq. (8) from Cry1Ab transport breakthrough curves (Fig. 3). Based on the transport breakthrough curves of Cry1Ab, the adsorption isotherms of Cry1Ab in zeolite and humic acid-coated zeolite were determined, which followed Langmuir adsorption isotherms:

$$S = \frac{\alpha K C_e}{1 + K C_e} \tag{9}$$

where S is the adsorbed Cry1Ab in zeolite, α is the mass of Cry1Ab required to completely cover a unit mass of zeolite, C_e is the Cry1Ab equilibrium concentration, and K is the Langmuir adsorption constant, which increases with the increase of the binding energy of adsorption. The α and K values were obtained using numerical simulation of the Langmuir adsorption isotherms (Fig. 4). CrylAb had α value of 0.073 ng/g for ZK406H, 0.135 ng/g for ZS403H, and 0.037 ng/g for ZS500H. With humic acid coating, the α values decreased to 0.057, 0.086, and 0.036 ng/g, respectively. α exponentially increased with the increase of zeolite clay-specific surface area (Fig. 5). The K values had opposite trends as compared to α, which increased from 246, 89, and 42 to 421, 105, and 71 mL/ng for ZK406H, ZS403H, and ZS500H, respectively, with humic acid coating. The underlying principle behind the adsorption isotherms resulted from forms of bonding between Cry1Ab and adsorption receptor sites on zeolite

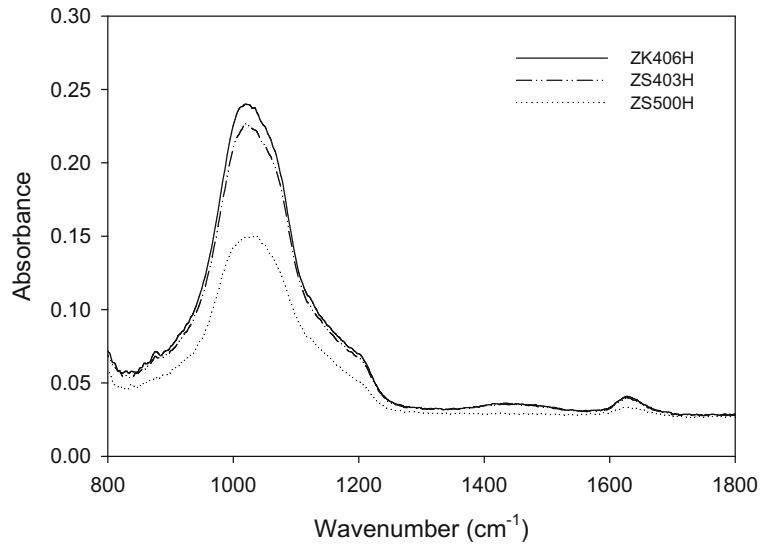

Fig. 7 Zeolite surface functional groups determined by infrared spectroscopy

surfaces. Therefore, the coating of humic acids changed the bonding energy between Cry1Ab and the adsorption receptor sites on zeolite surfaces. The K values were linked to the partition coefficient of Cry1Ab between the aqueous phase and zeolite, K_p, which exponentially increased with the increase of K (Fig. 6).

To further understand the different behaviors of zeolite clays in terms interactions with Cry1Ab, infrared spectroscopy (IR) was performed to investigate the chemical structures of the zeolite clays. The IR results indicated that zeolite was mainly composed of ethers (−CH_2–O–, CH_3–O–, −C–O–C–) (peaks shown at the frequencies of 1000, 980, 1060 cm^{-1}) besides a much smaller amount of aldehydes (RCOH) (1700 cm^{-1}), ketones (RCOR) (1680 cm^{-1}), carboxylic acids (RCOOH and RCOO–) (1690 and 1600 cm^{-1}), and hydroxyl (OH–) (3600 cm^{-1}). Functional groups of ethers contributed to the surface hydrophobicity, and aldehydes, ketones, and carboxylic acids contributed to the surface hydrophilicity (Barnes et al. 1944). As shown in Fig. 7, ZK406H and ZS403H had much stronger peak intensities at the frequency of 1000 cm^{-1} than those of ZS500H. Consequently, ZK406H and ZS403H exhibited more surface hydrophobicity and stronger retention of Cry1Ab.

Funding Information The work was supported by the USDA National Institute of Food and Agriculture, Grant No. 2016-67020-25275, to Florida A&M University.

References

Bai, G., Brusseau, M. L., & Miller, R. M. (1997). Influence of a rhamnolipid biosurfactant on the transport of bacteria through a sandy soil. *Applied and Environmental Microbiology, 63*, 1866–1873.

Barnes, R. B., Gore, R. C., Liddel, U., & Williams, V. Z. (1944). *Infrared spectroscopy, industrial applications and bibliography*. New York: Reinhold Publishing Corporation.

Barton, J. E., & Dracup, M. (2000). Genetically modified crops and the environment. *Agronomy Journal, 92*, 797–803.

Burgisser, C. S., Cernik, M., Borkovec, M., & Sticher, H. (1993). Determination of nonlinear adsorption-isotherms from column experiments: an alternative to batch studies. *Environmental Science and Technology, 27*, 943–948.

Carstens, K., Anderson, J., Bachman, P., De Schrijver, A., Dively, G., Federici, B., Hamer, M., Gielkens, M., Jensen, P., Lamp, W., Rauschen, S., Ridley, G., Romeis, J., & Waggoner, A. (2012). Genetically modified crops and aquatic ecosystems: considerations for environmental risk assessment and non-target organism testing. *Transgenic Research, 21*, 813–842.

Clark, B. W., Phillips, T. A., & Coats, J. R. (2005). Environmental fate and effects of *Bacillus thuringiensis* (*Bt*) proteins from transgenic crops: a review. *Journal of Agricultural and Food Chemistry, 53*, 4643–4653.

Fu, Q. L., Zhang, Y. H., Huang, W., Hu, H. Q., Chen, D. Q., & Yang, C. (2012). Remaining dynamics of Cry1Ab proteins from transgenic *Bt* corn in soil. *Journal of Food Agriculture and Environment, 10*, 294–298.

Helassa, N., M'Charek, A., Quiquampoix, H., Noinville, S., Dejardin, P., Frutos, R., & Staunton, S. (2011). Effects of physicochemical interactions and microbial activity on the persistence of Cry1Aa *Bt* (*Bacillus thuringiensis*) toxin in soil. *Soil Biology and Biochemistry, 43*, 1089–1097.

Lehrman, A., & Johnson, K. (2008). Swedish farmers attitudes, expectations and fears in relation to growing genetically modified crops. *Environmental Biosafety Research, 7*, 153–162.

Loureiro, I., Escorial, C., Garcia-baudin, J. M., & Chueca, C. (2009). Hybridization, fertility and herbicide resistance of hybrids between wheat and *Aegilops biuncialis*. *Agronomy for Sustainable Development, 29*, 237–245.

Lutz, B., Wiedemann, S., & Albrecht, C. (2006). Degradation of transgenic Cry1Ab DNA and protein in *Bt*-176 maize during the ensiling process. *Journal of Animal Physiology and Animal Nutrition, 90*, 116–123.

Ma, L. W., Shaffer, M. J., Boyd, J. K., Waskom, R., Ahuja, L. R., Rojas, K. W., & Xu, C. (1998). Manure management in an irrigated silage corn field: experiment and modeling. *Soil Science Society of America Journal, 62*, 1006–1017.

Peterson, G., Cunningham, S., Deutsch, L., Erickson, J., Quinlan, A., Raez-Luna, E., Tinch, R., Troell, M., Woodbury, P., & Zens, S. (2000). The risks and benefits of genetically modified crops: a multidisciplinary perspective. *Conservation Ecology, 4*, 1–13.

Reed, K. W. (1965). On a problem in neutron transport theory. *Journal of Mathematical Analysis and Applications, 10*, 161–165.

Toride, N. L., Leij, F. J., & van Genuchten, M. T. (1995). *The CXTFIT code for estimating transport parameters from laboratory or field experiments, version 2.1*. Riverside: U.S. Salinity Laboratory.

Unice, K. M., & Logan, B. E. (2000). Insignificant role of hydrodynamic dispersion on bacterial transport. *Journal of Environmental Engineering, 126*, 491–500.

Uzogara, S. G. (2000). The impact of genetic modification of human foods in the 21st century: a review. *Biotechnology Advances, 18*, 179–206.

Wheatley, R. (2009). Impact of genetically modified crops on soil and water ecology. In N. Ferry & A. M. R. Gatehouse (Eds.), *Environmental impact of genetically modified crops* (pp. 225–239). Oxfordshire: CABI.